Journal of Chromatography A, 1218 (2011) 1519–1529

Contents lists available at ScienceDirect

Journal of Chromatography A

journal homepage: www.elsevier.com/locate/chroma

Adsorption of deamidated antibody variants on macroporous and dextran-grafted cation exchangers: I. Adsorption equilibrium

Yinying Tao [a], Giorgio Carta [a,*], Gisela Ferreira [b], David Robbins [b]

[a] Department of Chemical Engineering, University of Virginia, 102 Engineers' Way, Charlottesville, VA 22904-4741, USA
[b] MedImmune, One MedImmune Way, Gaithersburg, MD 20877 USA

ARTICLE INFO

Article history:
Received 29 October 2010
Received in revised form 13 January 2011
Accepted 17 January 2011
Available online 22 January 2011

Keywords:
Monoclonal antibody charge variants
Deamidation
Adsorption isotherm
Ion exchange
Selectivity
Linear gradient elution

ABSTRACT

Single and multicomponent adsorption isotherms were obtained for deamidated variants of a monoclonal antibody on two cation exchangers with different pore structures, one with a macroporous architecture – UNOsphere S, and the other with charged dextran grafts – Capto S. No selectivity between the different deamidated forms was seen at pH 5 for either stationary phase. However, although the binding strength was lower, both media exhibited substantial selectivity at pH 7.5. The effective binding charge, determined from linear gradient elution experiments and from the steric mass action model, was different for the two different media, but remained nearly the same for the different variants suggesting that the selectivity is determined by the strength of binding, rather than by the binding charge. This result agrees with the higher binding constants determined for the less deamidated forms. At low ionic strength, the binding capacity of the dextran grafted media was much higher than that of the macroporous matrix at either pH. However, similar capacities were obtained for the two stationary phases at ~140 mM Na^+ for pH 5 and at 50 mM Na^+ for pH 7.5. For both materials, predictions of multicomponent adsorption based on the steric mass action model were in good agreement with experimental results indicating that the different variants bind in competition with each other. In general, this work demonstrates the utility of modeling adsorption equilibrium allowing an accurate description of competitive binding, which is a necessary step for a complete description of a chromatographic separation process.

1. Introduction

Deamidation has been shown to occur post-translationally in a variety of therapeutic antibodies and other protein-based pharmaceuticals [1–3]. Such modifications introduce charge and structural heterogeneity, which, in turn, may impact activity and stability of the protein [4–6]. While in some cases altering upstream processing can reduce the charge variants, downstream processing is often necessary to separate and remove them.

Analytical ion exchange chromatography (IEC) has been commonly used to quantitate protein charge variants [7–9]. Examples are the resolution of N-terminus analogues of recombinant human interleukin-1β [10], of C-terminus variants of monoclonal antibodies (mAbs) [12] and of deamidated variants of mAbs [13]. Besides applying IEC as an analytical tool there is a growing interest in its preparative use. However, most of the published work has been done with analytical-sized particles and at very low-loading conditions. For example, Adachi et al. [11] used 5 μm diameter MCI Gel ProTex ion exchangers to separate protein isoforms with 12 μg/ml loads. Weitzhandler et al. [12] and Melter et al. [9] used 10 μm diameter ProPac WCX-10 and SCX-10 to resolve antibody charge variants, but protein loads and operating pressure on these pellicular adsorbents were still far from those acceptable for industrial uses. Thus, there is a need to understand the adsorption of antibody charge variants for preparative conditions that are relevant to industrial practice.

The optimized design of chromatographic separation processes normally requires a balance between productivity (mass antibody processed per volume of packed gel per time) and resolution, which is affected by adsorption equilibrium, mass transfer, and flow characteristics. Adsorption equilibrium is normally considered first because it determines the ideally achievable separation. Many studies have addressed the measurement and description of single component protein adsorption. However, only a few authors have addressed multicomponent systems for high loading conditions despite the fact that their description is needed to predict protein separation under non-linear conditions. Prior work in this area has been devoted primarily to model proteins. Skidmore and Chase [14] considered the adsorption of BSA and lysozyme on the cation exchanger S-Sepharose-FF and found that a competitive Langmuir type model could describe the two-component adsorption behavior but found that predictions based on single-component data

* Corresponding author. Tel.: +1 434 924 6281; fax: +1 434 982 2658.
E-mail address: gc@virginia.edu (G. Carta).

0021-9673/$ – see front matter © 2011 Elsevier B.V. All rights reserved.
doi:10.1016/j.chroma.2011.01.049

Nomenclature

Symbols

C	fluid phase concentration (mg/ml or mM)
C_I	Na^+ concentration (mM)
C_I^R	Na^+ concentration at which peak elutes (mM)
CV	effluent volume divided by column volume
$\bar{d}_p$	mean particle diameter (μm)
k'	retention factor
K_e	equilibrium constant for protein-counterion exchange
L	column length (cm)
q	adsorbed phase concentration (mg/ml or mM)
q_0	charge density of stationary phase (mM or μmol/ml)
r_m	solute hydrodynamic radius (nm)
r_{pore}	pore radius (nm)
t_G	gradient duration (s)
v	interstitial mobile phase velocity (cm/s)
V	solution volume (ml)
V_M	volume of particles (ml)
z	protein effective binding charge
ε	extraparticle porosity
ε_p	total intraparticle porosity
ε_{pM}	intraparticle macroporosity
$\alpha_{i,j}$	selectivity between components i and j
γ	normalized gradient slope (mM) = $(C_I^f - C_I^0)L/vt_G$
ϕ	phase ratio = $(1-\varepsilon)/\varepsilon$
σ	hindrance factor in SMA model

Subscripts

i	component number

Superscripts

f	final value
0	initial value

were rather inaccurate. Lewus and Carta [15] considered both simultaneous and sequential adsorption of cytochrome *c*–lysozyme mixtures on composite silica-polyacrylamide cation exchangers and found that two-component binding could be described by the multicomponent steric mass action (SMA) model of Brooks and Cramer [16]. Garke et al. [17] studied the simultaneous adsorption of γ-globulin and lysozyme on the cation exchanger Streamline SP. In this case, the smaller protein lysozyme was preferentially adsorbed and displaced γ-globulin, while γ-globulin had little or no effect on binding of lysozyme. A model based on a modified form of the multicomponent Langmuir isotherm and accounting for the different molecular sizes of the two proteins developed by Gu et al. [18] was used to describe the two-component isotherm. Recently, El-Sayed and Chase [19] used a competitive Langmuir model to describe simultaneous adsorption of α-lactalbumin and α-lactoglobulin on SP-Sepharose-FF while Xu and Lenhoff [20] showed that binary adsorption of model proteins on various cation-exchange media could be described based on a colloidal-energetic model using single-component isotherm parameters.

In this work, the adsorption behavior of mAb deamidated variants on two structurally different cation exchangers – UNOsphere S and Capto S – was studied for both single and multicomponent systems. According to their respective manufacturers, the former consists of rigid macroporous polymer-based particles while the latter is a crosslinked agarose matrix with charged dextran polymer grafts. These commercially available matrices for industrial bioprocess chromatography typify two different structures that can result in potentially different binding mechanisms. Protein binding in UNOsphere S is thought to occur on the surface of the relatively large pores of the support matrix. On the other hand, protein binding on Capto S is thought to occur on the flexible dextran grafts, which, in turn, can give greater accessibility to the charged ligands and, hence, higher capacity [21]. In Part I of this work, we cover the basic properties of the stationary phases, the relevant properties of the mAb charge variants, and their single and multicomponent adsorption equilibrium using both batch isotherms and linear gradient elution chromatography. In Part II, we cover the kinetics of single and multicomponent adsorption.

2. Experimental

2.1. Materials

The two cation exchangers used in this work are UNOsphere S, obtained from Bio-Rad Laboratories (Hercules, CA, USA), and Capto S, obtained from GE Healthcare (Piscataway, NJ, USA). Characterization of charge density by titration, particle size distribution (PSD) by microphotography, and accessible pore size by inverse size exclusion chromatography (iSEC) with glucose and dextran standards were performed for these two matrices as described in detail by Tao and Carta [22].

A mAb with molecular mass ~150 kDa and pI ~ 8.9, determined by non-reducing SDS-PAGE and isoelectric focusing, respectively, was obtained from MedImmune (Gaithersburg, MD, USA), and used to generate deamidated forms as described in Section 2.2.1. All chemicals and reagents were purchased from Fisher Scientific (Pittsburgh, PA, USA). Adsorption experiments were done at room temperature, 22 ± 2 °C.

2.2. Methods

2.2.1. Preparation of mAb deamidated forms

Deamidated variants were obtained by sequentially exchanging a stock protein sample against 1 M Tris buffer at pH 9.5 with a PD 10 SEC column (Fisher Scientific) and keeping the solution for 10 days at room temperature. The process was terminated by exchanging the protein sample against 10 mM Na_2HPO_4 pH 7.5 buffer. The deamidated variants produced by this process were then separated at pH 7.5 with a 10 mm × 100 mm Source 30S column (GE Healthcare) using a segmented salt gradient from 0 to 150 mM NaCl at 2 ml/min. The fractions pooled from several replicate runs were concentrated and dialyzed against 10 mM Na_2HPO_4, pH 7.5 using a stirred ultrafiltration cell (Fisher Scientific), and finally stored at −20 °C for future use.

2.2.2. Isoelectric focusing

Isoelectric focusing (IEF) was performed with a Multiphor II unit (GE Healthcare) according to the equipment manufacturer instructions. Briefly, an Isogel agarose plate with a pH gradient from 7 to 11 (Fisher Scientific) was placed in the center of the apparatus platform. Cathode and anode wicks were then placed at the negative and positive electrode contact of the gel. A sample applicator mask was placed across the gel approximately 3 cm from the anode wick, and 10 μg of samples and pI markers (Fisher Scientific) were then loaded on the applicator slots. The power limit was set at 1 W for 10 min to prefocus the samples. Then the applicator mask was removed and the power limit was increased to 25 W to continue focusing for 90 min. The focused gel was fixed in a solution containing 36% (v/v) methanol, 3.6% (w/v) sulphosalicylic acid and 6% (w/v) tricholoacetic acid, washed with deionized water and finally stained with GelCode blue stain reagent (Thermo Scientific) and washed with deionized water again.

2.2.3. Analytical cation exchange chromatography

Analytical cation exchange chromatography was conducted with a Waters HPLC system (Milford, MA) with a 4 mm × 250 mm Propac WCX-10 column (Dionex Corporation, Sunnyvale, CA, USA) to characterize the mAb charge variants using mobile phases containing 10 mM Na_2HPO_4 at pH 7.5 (buffer A) and 10 mM Na_2HPO_4 containing 100 mM NaCl at pH 7.5 (buffer B). Samples containing approximately 0.1 mg protein were injected into the column and eluted at 1 ml/min with a 20–80% B linear gradient for 6.4 column volumes (CV) followed by a strip at 100% B.

2.2.4. Linear gradient elution

Gradient elution was used to determine the equilibrium parameters of each mAb fraction in the low loading limit. In these experiments, 100 μl samples containing 3 mg/ml of each mAb variant was injected to 10 mm × 100 mm UNOsphere S and Capto S columns and eluted with gradients with varying durations and different initial and final NaCl concentrations in 10 mM Na_2HPO_4 at pH 7.5. The mobile phase flow rate was kept constant at 2.5 cm/min and 1.25 cm/min for UNOsphere S and Capto S, respectively. In each case, the Na^+ concentration at peak elution, C_I^R, was determined from the conductivity at the CV corresponding to the first moment of each eluted peak.

2.2.5. Adsorption isotherms

Adsorption isotherms were obtained in 20 mM sodium acetate adjusted to pH 5.0 with acetic acid and in 10 mM Na_2HPO_4 adjusted to pH 7.5 with phosphoric acid. Solutions with various ionic strengths were prepared by adding sodium chloride to each base buffer prior to pH adjustment.

Single-component isotherms were obtained by mixing known amounts of hydrated particles with a series of protein solutions at different concentrations with a ratio of particle and solution volumes estimated to yield a 50% drop in protein concentration. The mixture of media and protein solution was allowed to equilibrate for 24–48 h in test tubes rotated slowly end to end. After equilibration, the samples were centrifuged at 5000 rpm for 5 min, and the supernatant analyzed spectrophotometrically at 280 nm to determine the residual protein concentration. For binary adsorption isotherms, samples were additionally analyzed by HPLC to determine the concentration of each isoform before and after equilibrium using a 5 mm × 50 mm Source 30S column with a 30 CV linear gradient from 25 to 60 mM NaCl in 10 mM Na_2HPO_4 adjusted to pH 7.5 with phosphoric acid at 1 ml/min. The percentage of each mAb fraction was determined by taking the ratio of peak areas. Finally, the adsorption capacity for individual mAb fractions was obtained by material balance.

3. Results and discussion

3.1. Properties of cation exchangers

A summary of the relevant material properties is given in Table 1. As seen in this table, UNOsphere S has a lower charge density and smaller average particle size than Capto S. However, more important structural differences are revealed by the iSEC results shown in Fig. 1. For UNOsphere S, all of the dextran standards with molecular masses between 10 and 500 kDa were separated and their retention varied only slightly with salt concentration indicating that this material contains relatively large macropores with a rigid structure. Conversely, for Capto S all dextran probes with

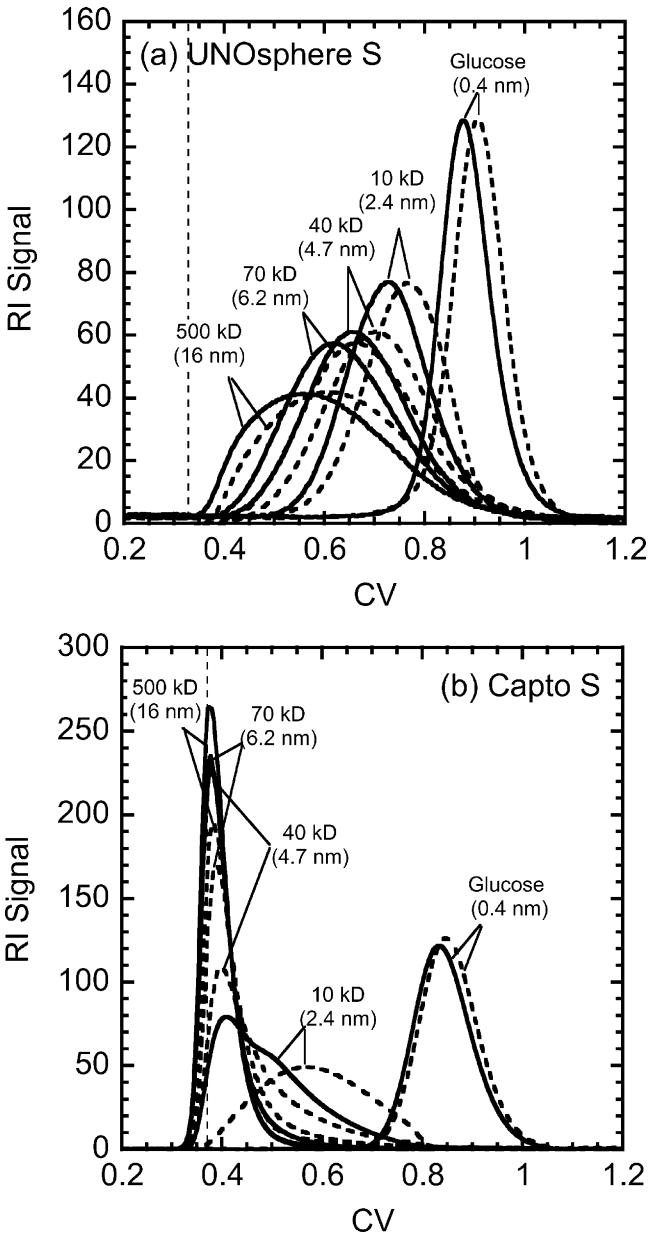

Fig. 1. Inverse size exclusion chromatography (iSEC) results for (a) UNOsphere S and (b) Capto S. Solid and dashed lines show refractive index (RI) detector traces for glucose and various dextran standards in 0 and 1 M NaCl, respectively. Vertical dashed line shows the extraparticle porosity. Values in parenthesis are the hydrodynamic radii calculated for the different molecular mass dextrans and glucose.

Table 1
Summary of stationary phase properties.

Matrix	q_0 (μmol/ml)	$\bar{d}_p$ (μm)	ε	ε_p[c]	ε_{pM}[d]	r_{pore} (nm) in 0 M NaCl[d]	r_{pore} (nm) in 1 M NaCl[d]
UNOsphere S	148 ± 4	75	0.33 ± 0.02[a]	0.80	0.59 ± 0.05	68 ± 20	74 ± 22
Capto S	220	89	0.37 ± 0.02[b]	0.74	ND	ND	ND

[a] Based on pressure drop and Karman–Cozeny equation in 0 M NaCl.
[b] Based on retention of blue dextran.
[c] Based on retention of glucose.
[d] Based on dextran exclusion.

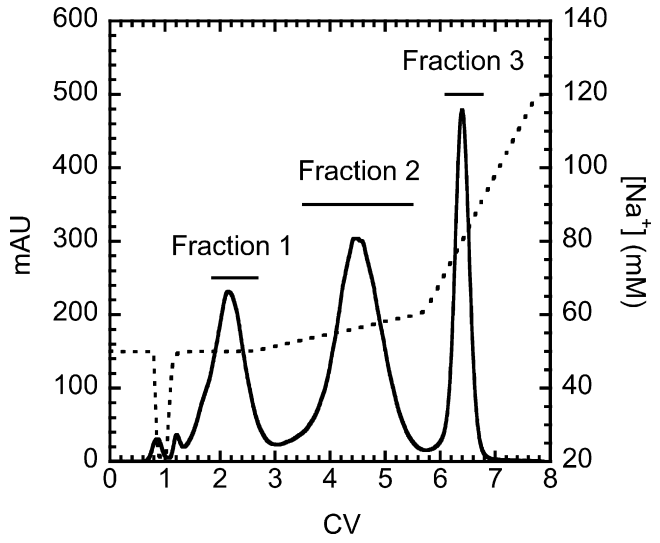

Fig. 2. Chromatogram of deamidated mAb mixture on 10 mm × 100 mm Source 30S column. Total protein injected = 17 mg. Horizontal bars indicate the fractions collected.

molecular mass of 40 kDa or larger co-eluted at low ionic strength and became only partially resolved in 1 M NaCl. The latter result is consistent with the behavior observed previously for other experimental and commercial dextran-grafted matrices [23,24]. Based on these data we surmise that at low ionic strengths, the surface-bound charged dextran grafts are extended into the pore space hindering transport of neutral macromolecules, while allowing glucose to diffuse freely. Partial collapse of these grafts occurs at higher ionic strengths as a result of shielding of repulsive intrachain and interchain electrostatic interactions. Porosities and pore radii could be obtained from these data for UNOsphere S and are shown in Table 1. The extraparticle porosity, ε, was determined from the column pressure drop according to the Karman–Cozeny equation and the total intraparticle porosity, ε_p, was obtained from the retention of glucose. Finally, the intraparticle macroporosity, ε_{pM}, and the apparent pore radius, r_{pore}, were obtained by fitting the dextran retention volumes based on a cylindrical pore model according to the following equation [23–25]:

$$\overline{CV} = \varepsilon + (1-\varepsilon)\varepsilon_{pM}\left(1 - \frac{r_m}{r_{pore}}\right)^2 \quad (1)$$

where $\overline{CV}$ is the peak retention volume normalized by the column volume and r_m is the dextran hydrodynamic radius. The latter was calculated as described elsewhere [23]. As seen in Table 1, the apparent pore size of UNOsphere S is more than ten times larger than the size of the mAb molecules ($r_m \sim 5$ nm), which should result in modest diffusional hindrance. A different result is obtained for Capto S. In this case, since only one of the dextran probes (10 kDa) could gain significant access to the interior of the particles, Eq. (1) could not be used reliably to determine ε_{pM} and r_{pore}. However, based on Fig. 1b, it is obvious that the size exclusion limit of Capto S for neutral probes is between 4.7 and 6.2 nm in 0 M NaCl and between 6.2 and 16 nm in 1 M NaCl. In either case, the exclusion limit is similar in magnitude to the mAb indicating that mAb binding and transport are likely to be affected strongly by interactions with the ionically functionalized dextran.

3.2. Properties of deamidated variants

Fig. 2 shows a representative chromatogram of the deamidated mAb mixture on Source 30S. Three major peaks were obtained and were collected as separate fractions identified as fractions 1, 2 and 3 in an approximate ratio of 1:2:1. Since deamidation converts asparagine and (to a lesser extent) glutamine residues to carboxylic acid groups that are negatively charged at pH 7.5, the deamidated variants are expected to elute earlier.

Analyses of the three fractions collected from the Source 30S column were conducted by Propac cation exchange and IEF. Fig. 3 shows the overlaid chromatograms of the three mAb fractions and the corresponding IEF results. The chromatogram for the unmodified protein is also shown. The order of elution was the same as that obtained with the Source 30S column. However, the Propac column resolved multiple subspecies resulting in three major peaks for each fraction. Based on the IEF results each fraction gave rise to three major bands spanning a 0.2-unit pI-range as summarized in Table 2. The multiple bands within each fraction were likely due to the availability of multiple deamidation sites on the mAb pep-

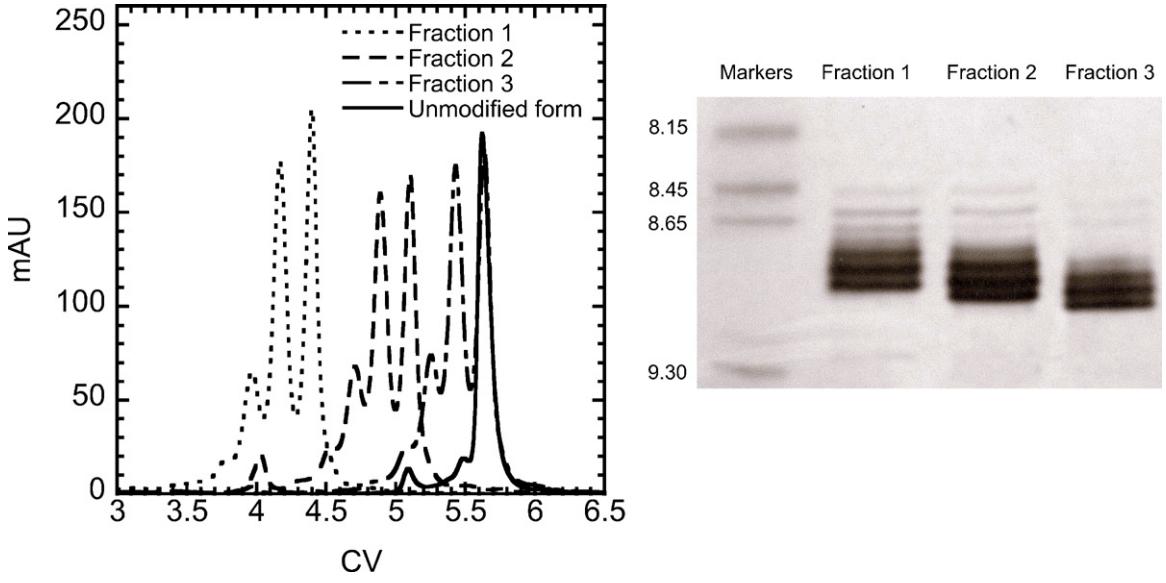

Fig. 3. Overlaid chromatograms of mAb fractions on Propac WCX-10 column. Injection amounts: 125 μg for each fraction and 60 μg for unmodified protein. Note that the late eluting peak from fraction 3 coincides with that of the unmodified protein (suggesting that the fraction contains a portion of non-deamidated protein). Panel on right shows the corresponding IEF analyses.

Table 2
Characteristics of mAb isoforms in fractions collected from Source 30S column.

mAb fraction	pI range[a]	Net charge difference from native form at pH 7.5[b]
1	8.69–8.90	−2.5
2	8.73–8.96	−1.6
3	8.80–9.00	−0.74

[a] Based on IEF analyses.
[b] Based on Figs. 3 and 4.

tide chains. Vlasak et al. [26] showed similar results for another deamidated mAb and attributed the multiple peaks to combinations of deamidation in the mAb variable and constant regions. A simple hypothetical model shown in Fig. 4 is consistent with our data. The model assumes that there are multiple deamidation sites that affect retention greatly resulting in "major" isoforms that are resolved with the Source 30S column and additional deamidation sites that affect retention much less strongly and that result in subspecies that can only be separated with the Propac column. Based on this qualitative model and the relative peak areas obtained with the Propac column we can calculate the average net charge change of each fraction relative to the native mAb. The results are summarized in Table 2. In practice, only the major isoforms were resolved with the preparative-sized resins used in this work. Thus, the subspecies are expected to have little influence on the adsorptive behavior on Capto S and UNOsphere S. As a result, each mAb fraction was treated as a single pseudo-component. A similar approach has been presented by Forrer et al. [27]. These authors showed that the chromatographic behavior of a highly heterogeneous polyclonal antibody could be represented with a few pseudo-components, each of which lumped together closely related charge variants that did not vary greatly in retention properties.

3.3. Gradient elution behavior

Fig. 5 shows the linear gradient elution (LGE) profiles obtained with different gradient slopes for mAb fraction 3 at pH 7.5. The behavior was qualitatively similar for each of the other fractions and for the unmodified protein (results not shown). The conductivity traces were linear for each case. For both chromatographic media, the peaks eluted at higher Na^+ concentration values (C_I^R) when the gradient slope was higher. The peaks obtained for UNOsphere S were nearly symmetrical within a wide range of gradient slopes. However, the Capto S peaks exhibited a distinct tail and were much broader than those obtained for UNOsphere S under similar gradient slopes. A possible explanation of this result is that significant diffusional hindrance exists in the Capto S particles for these conditions. Another possibility, however, is that non-specific binding caused tailing due to non-linear adsorption despite the high Na^+ concentration. Some experiments were also carried out at pH 5.0 (results not shown). Under this condition, there was no selectivity between the different mAb fractions, likely because at this pH most of the deamidated residues are protonated and thus uncharged and the corresponding small charge differences are relatively insignifi-

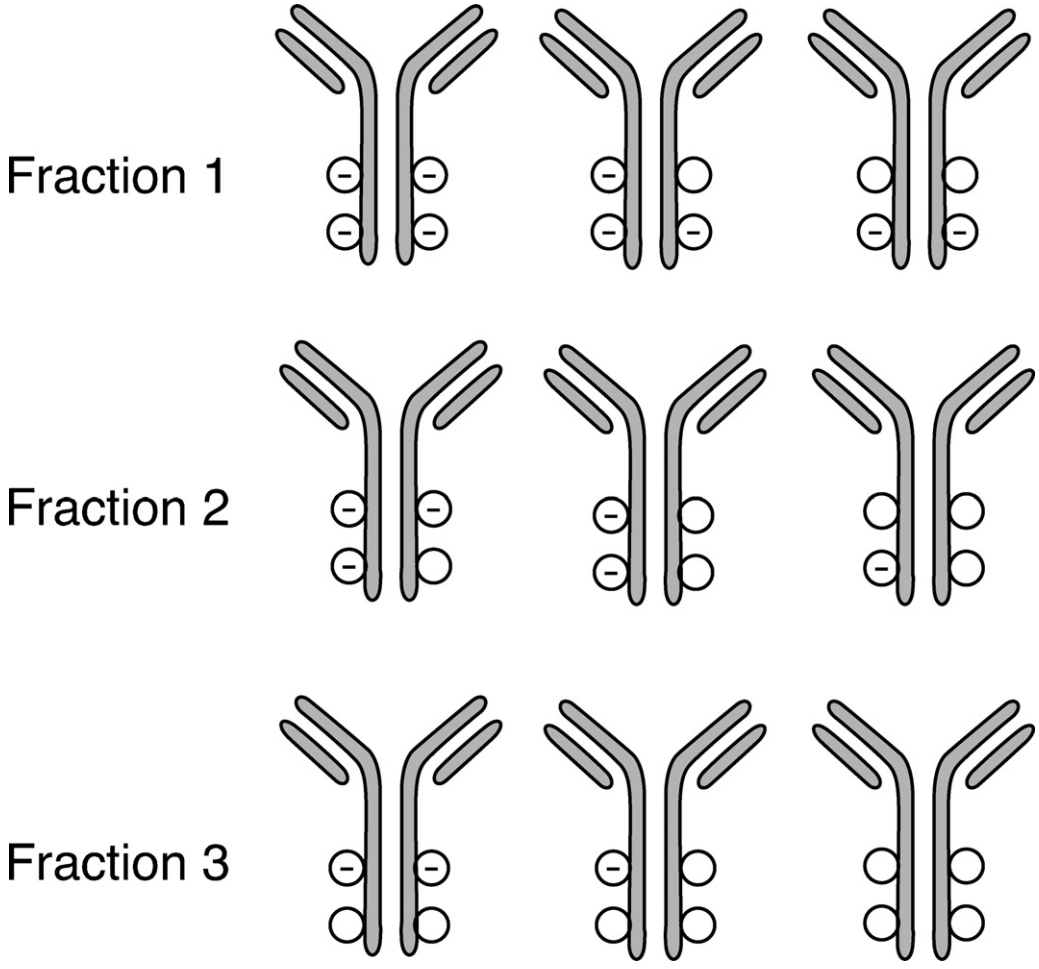

Fig. 4. Sketch of putative deamidated variants. Each row corresponds to the "major" peaks resolved on the Source 30S column and collected as fractions 1, 2, and 3, respectively. Sketches in each row correspond to the "minor" variants resolved on the Propac column. Circles represent deamidation sites. Circles with dashes are deamidated residues. The actual location of the deamidation sites shown is fictitious.

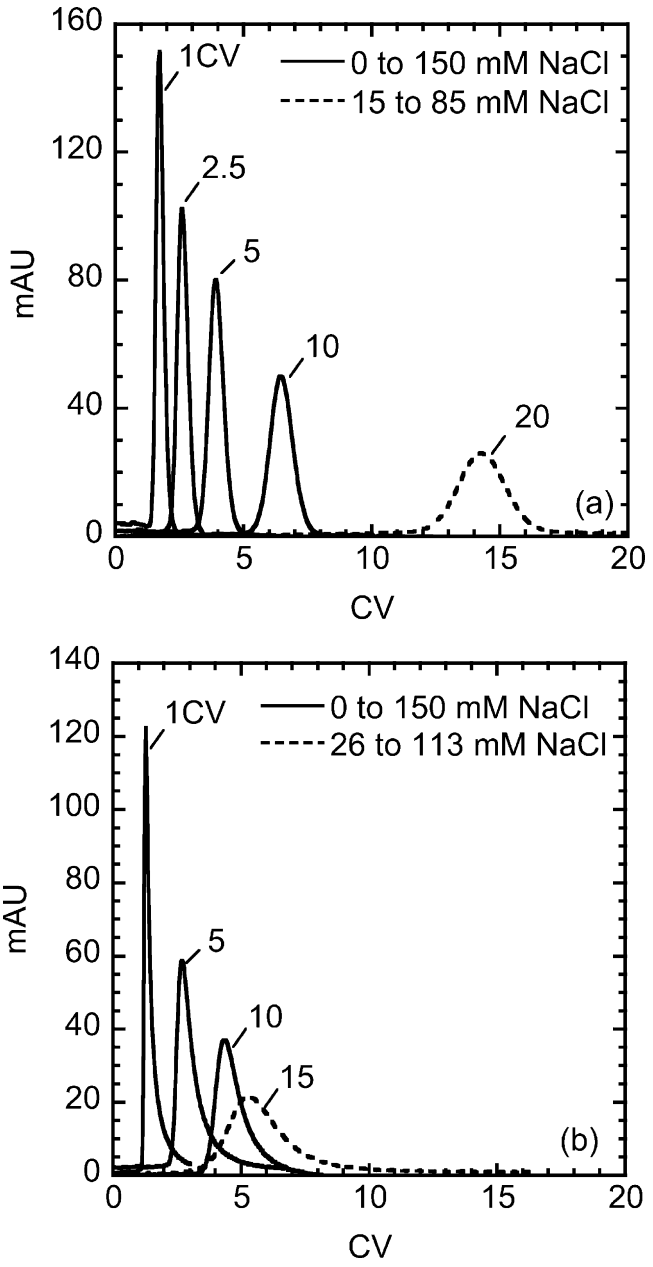

Fig. 5. Overlaid linear gradient elution (LGE) chromatograms of mAb fraction 3 for (a) UNOsphere S and (b) Capto S. Mobile phase was 10 mM Na_2HPO_4 at pH 7.5 with different initial and final NaCl concentrations and gradient durations (CV units) as indicated in the figure legends.

cant in comparison with the overall net charge at this pH, which is very far from the isoelectric point.

Based on the steric mass action (SMA) model for an *n*-component system [28], protein binding on a cation exchanger is described by the following implicit equation:

$$q_i = K_{e,i}\left[\frac{q_0 - \sum_1^n (z_i+\sigma_i)q_i}{C_I}\right]^{z_i} C_i \quad (2)$$

where q_0 is the charge density of the stationary phase, q_i and C_i are the adsorbed and liquid phase protein concentrations, respectively, C_I is the Na^+ counterion concentration, z_i is the protein effective binding charge, $K_{e,i}$ is the adsorption equilibrium constant for the exchange of protein and Na^+, and σ_i is the steric hindrance factor. At low protein loadings, when $\sum_1^n (z_i+\sigma_i)q_i \ll q_0$, this equation reduces to:

$$q_i = K_{e,i}\left(\frac{q_0}{C_I}\right)^{z_i} C_i \quad (3)$$

In this case, the retention factor, k_i', can be expressed as follows:

$$k_i' = \phi\left[\varepsilon_{p,i} + K_{e,i}\left(\frac{q_0}{C_I}\right)^{z_i}\right] \quad (4)$$

where $\phi = (1-\varepsilon)/\varepsilon$ is the phase ratio and $\varepsilon_{p,i}$ is the protein-accessible intraparticle porosity. Accordingly, the Na^+ concentration at which each protein elutes, C_I^R, is related to the normalized gradient slope $\gamma = (C_I^f - C_I^0)L/\nu t_G$ by the following equation [29]:

$$C_I^R = [\phi(z_i+1)K_{e,i}q_0^{z_i}\gamma + (C_I^0)^{z_i+1}]^{1/(z_i+1)} \quad (5)$$

where C_I^0 and C_I^f are the initial and final Na^+ concentrations, L the column length, ν the interstitial mobile phase velocity, and t_G the gradient duration. In practice, since C_I^0 is small and z_i is large, this equation is approximated by:

$$C_I^R \sim [\phi(z_i+1)K_{e,i}q_0^{z_i}\gamma]^{1/(z_i+1)} \quad (6)$$

Thus, plots of $\ln\gamma$ vs. $\ln C_I^R$ yield a straight line with slope z_i+1 and intercept $-\ln[\phi(z_i+1)K_{e,i}q_0^{z_i}]$. These plots are shown in Fig. 6 for the pH 7.5 data. Although substantial scatter exists, the plots are indeed linear for each mAb fraction. Although the scatter may be due, in part, to the presence of multiple subspecies, the main reason is the strong dependence of retention on salt concentration, which is typical for protein ion exchange [16]. Despite the fact that the net charge is different for the different mAb variants, the slopes and, hence, the *z*-values are very similar for all three, although they are different for the two chromatography media. The regressed values of *z* and K_e are summarized in Table 3. *z* could be determined with relative accuracy. As indicated by the estimated errors of the regressed parameters there is no statistically significant difference among the *z*-values for the three fractions, although the *z*-values are clearly higher for Capto S than for UNOsphere S. On the other hand, the regressed K_e-values have very large estimated errors. Nevertheless, the mean values show a decreasing trend with increasing deamidation. These results suggest that the negative charges brought about by deamidation affected the binding affinity, as indicated by the decreasing K_e values, but did not directly affect the effective binding charge. According to the SMA model, the latter represents the number of resin functional groups with which the protein interacts. This number did not change for different levels of deamidation but was higher for Capto S likely due to increased accessibility to ligands provided by the charged dextran grafts. Note that for these conditions, each mAb variant apparently gained access to the interior of the particles, even though for similar conditions neutral dextran probes of comparable hydrodynamic radius were completely excluded in Capto S. This result is similar to what has been reported previously for other dextran-grafted cation exchangers [23,24] and suggests that the dextran grafts have a highly dynamic structure whose fluctuations permit protein binding to occur when the electrostatic interaction is sufficiently strong despite the very low size exclusion limit for neutral dextran polymers.

3.4. Adsorption isotherms

3.4.1. Single component results

Adsorption isotherms were obtained at pH 5 and 7.5 and different salt concentrations. As in the gradient elution experiments, at pH 5.0 there was no difference in adsorption behavior for the different mAb fractions. Thus only the results for fraction 3 at pH 5 are included here and are shown in Fig. 7. For these conditions, the adsorption capacity was very high for Capto S exceeding 350 mg/ml

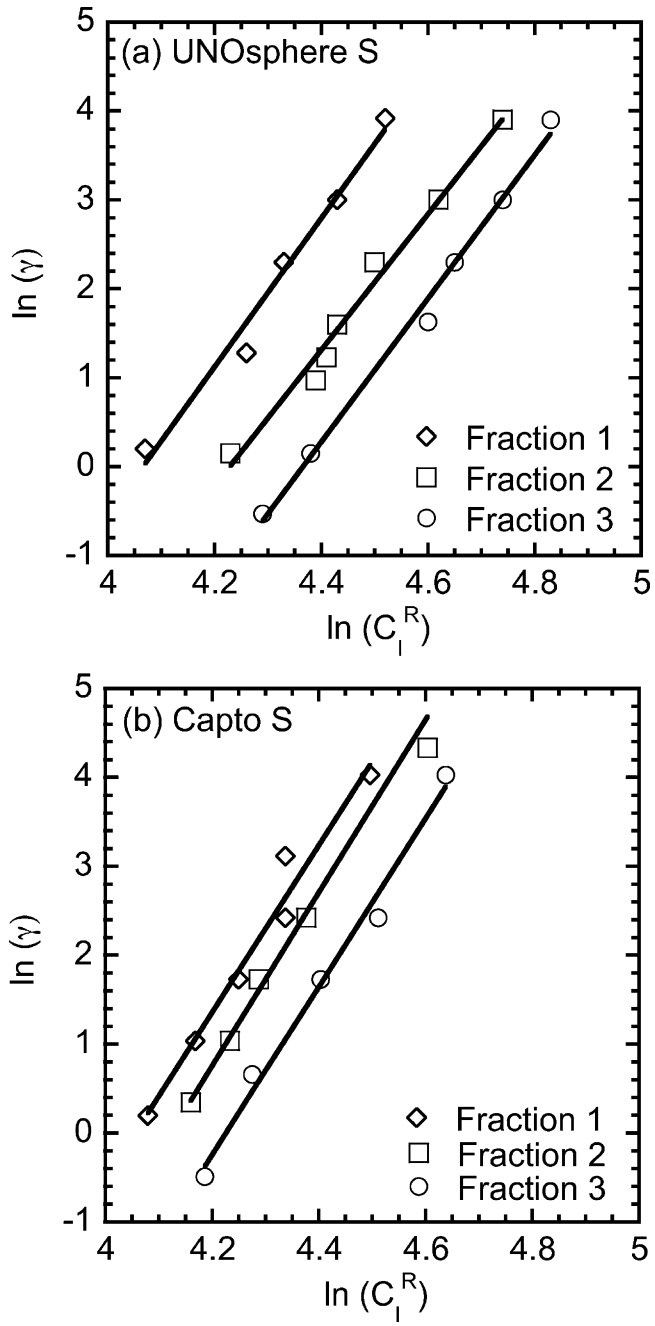

Fig. 6. LGE retention data plotted according to Eq. (6) for (a) UNOsphere S and (b) Capto S at pH 7.5. C_I^R is the Na^+ concentration at elution in mM units. γ is the normalized gradient slope (see text), also in mM units.

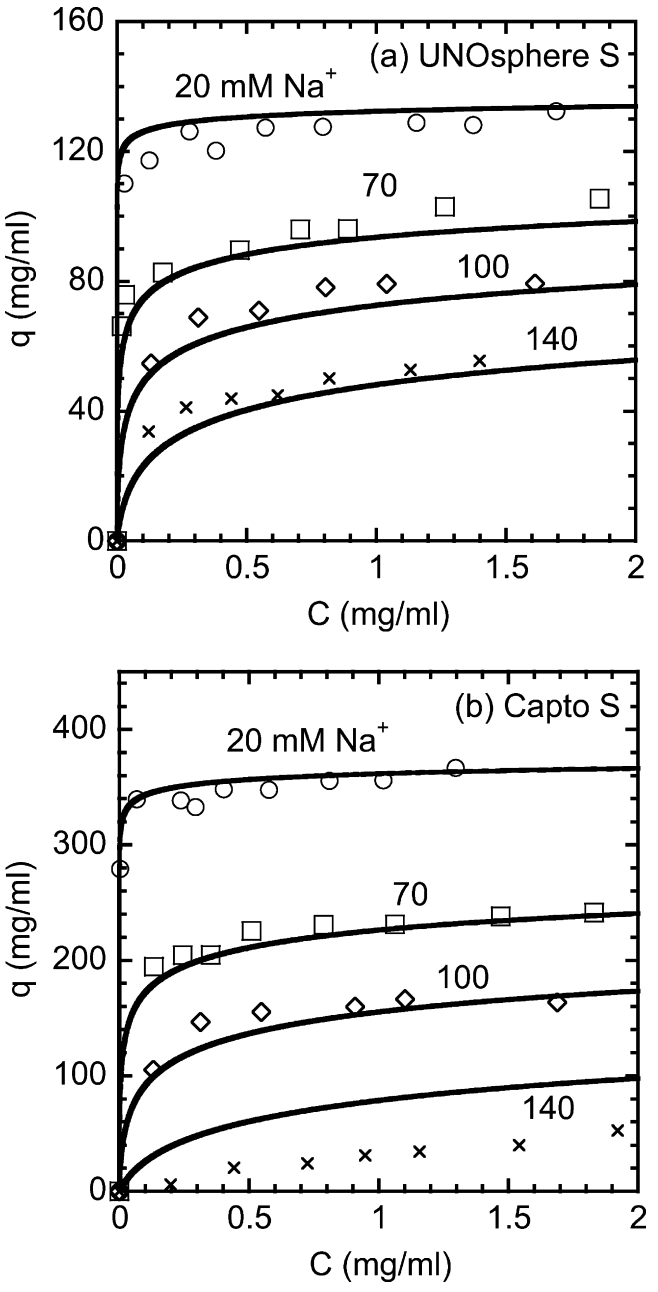

Fig. 7. Adsorption isotherms for mAb fraction 3 at pH 5.0 for (a) UNOsphere S and (b) Capto S. Lines are based on the SMA model.

Table 3
Summary of SMA isotherm parameters.

pH	Variant	Parameters	UNOsphere S LGE	Isotherms	Capto S LGE	Isotherms
7.5	1	z	7.36 ± 0.69	7.00	8.47 ± 0.61	8.26
		K_e ($\times 10^{-3}$)	3.63 ± 36.5	4.28 ± 0.23	0.047 ± 0.81	0.0084 ± 0.0003
		σ	–	122 ± 10	–	69.2 ± 7.1
	2	z	6.64 ± 0.45	7.00	7.91 ± 0.35	8.26
		K_e ($\times 10^{-3}$)	26.7 ± 102	36.8 ± 2.8	0.16 ± 0.37	0.11 ± 0.01
		σ	–	122 ± 10	–	69.2 ± 7.1
	3	z	7.07 ± 0.34	7.00	8.42 ± 0.83	8.26
		K_e ($\times 10^{-3}$)	55.4 ± 130	154 ± 14	0.22 ± 1.62	0.54 ± 0.03
		σ	–	122 ± 10	–	69.2 ± 7.1
5.0	3	z	ND	7.00	ND	8.26
		K_e ($\times 10^{-3}$)	ND	1054 ± 125	ND	10.4 ± 1.1
		σ	–	140 ± 10	–	69.2 ± 7.1

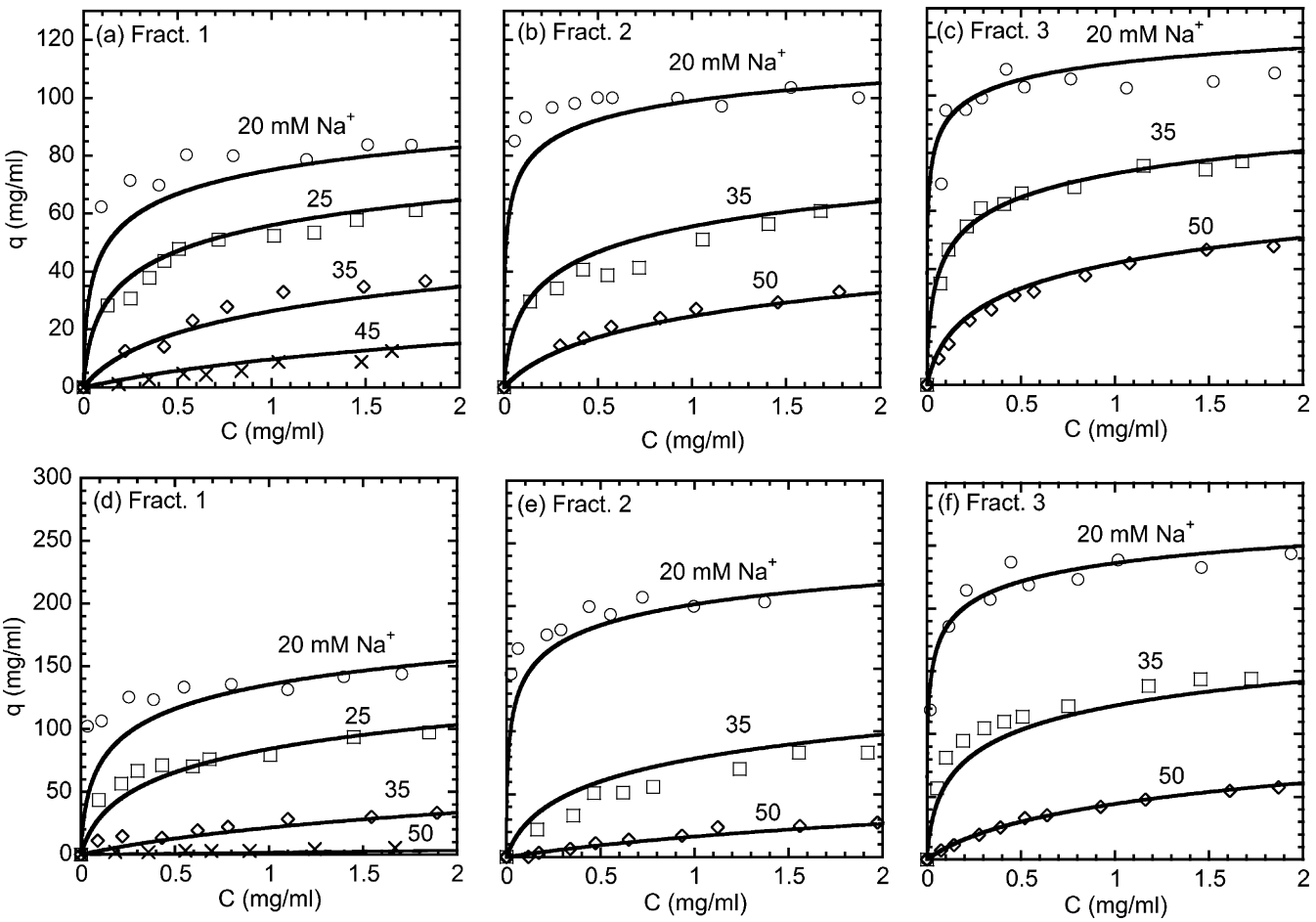

Fig. 8. Single component adsorption isotherms of mAb fractions 1, 2, and 3 at pH 7.5 on UNOsphere S (a–c) and Capto S (d–f). Lines are based on the SMA model. Note that different vertical scales have been used for UNOsphere S and Capto S.

of particle volume with 20 mM Na^+. Although both stationary phases show dependency of adsorption on salt concentration, the Capto S adsorption capacity was substantially more dependent than that of UNOsphere S. For example, at 140 mM Na^+ (corresponding to a conductivity of about 15 mS/cm at 20 °C), binding capacities at 2 mg/ml became nearly the same for the two matrices, but the binding strength (measured by the initial slope of the isotherm) became higher for UNOsphere S.

The results at pH 7.5 are shown in Fig. 8. In this case, different results were obtained for each mAb fraction with capacity and binding strength decreasing as the extent of deamidation increased. For all three fractions, binding was weaker than at pH 5.0 and was much more sensitive to salt concentration for both stationary phases. This behavior is in agreement with the lower overall charge of the mAb molecules at this pH, which is closer to the pI of the deamidated variants. The reduction in capacity caused by going from pH 5 to pH 7.5 was greater for Capto S compared to UNOsphere S. For example, for mAb fraction 3 at 20 mM Na^+, the maximum binding capacity decreased by about 30% for Capto S, but by only about 15% for UNOsphere S. At 50 mM Na^+ and pH 7.5, the binding capacity of UNOsphere S became larger than that of Capto S.

The SMA model given by Eq. (2) was used to fit the data. The model has three parameters, z, K_e, and σ, but the degree of correlation among them encountered in regressing the data was high. Thus, in order to reduce the degree of freedom, we used the average value of z determined from the LGE experiments and regressed the equilibrium constant K_e for each mAb variant while using the same regressed value of σ for all. Calculations were done using the advanced data fitting function in OriginPro 7.5 software (OriginLab Corporation, Northampton, MA, USA), which uses a Levenberg–Marquardt algorithm. The regressed parameters are in Table 3 along with their estimated errors. As expected, the relative accuracy of K_e obtained by regressing the isotherms is much greater than that obtained from the LGE data. Calculated curves given in Figs. 7 and 8, show that the SMA model could provide a reasonable fit of the isotherms with average relative deviation of ±10.5% for UNOsphere S and ±11.6% for Capto S at pH 7.5. Similar deviations were observed at pH 5, with the exception of the 140 mM NaCl Capto S data where little binding was observed.

As seen from Table 3, for both stationary phases the equilibrium constants determined by regression of the isotherms were similar to those determined by linear gradient elution (LGE), and in both cases decreased substantially as the extent of deamidation increased. This result indicates that the way the mAb molecules interacted with the stationary phase was the same for both low and high loading conditions. In both cases, the selectivity appeared to be determined not by the net charge (which is different for the different mAb fractions), but by the different affinities of the differently charged variants for the stationary phases. The larger z-values and the smaller σ-values obtained for Capto S are also consistent with the structural characteristics of this material where the charged dextran grafts presumably provide greater accessibility and more extensive interaction with the protein. However, at the same time, the larger z-values gave rise to a stronger dependence on the Na^+ concentration. The pH 5 parameter values also support these observations. At this lower pH, the positive protein charge increased

dramatically. Yet, for UNOsphere S only the equilibrium constant, K_e, increased dramatically indicating that protein-surface interactions were similar in number but stronger in magnitude when the net charge of the protein was higher. A similar result is seen for Capto S.

3.4.2. Multicomponent results

Fig. 9 shows the two-component isotherms for mixtures of mAb fractions 2 and 3 at pH 7.5 and various salt concentrations. These data were obtained with a constant ratio of initial protein concentrations of 1:3 for mAb fractions 2 and 3. Additional data for 20 mM Na^+ are shown in Table 4 for two and three-component systems with different initial ratios of the deamidated forms. Both stationary phases preferentially adsorbed mAb fraction 3 at all protein and salt concentrations. This result is consistent with the stronger protein-surface interactions of this variant seen from single-component adsorption data.

The multicomponent SMA model, Eq. (2), was applied to predict the multicomponent isotherms. Calculations where done by

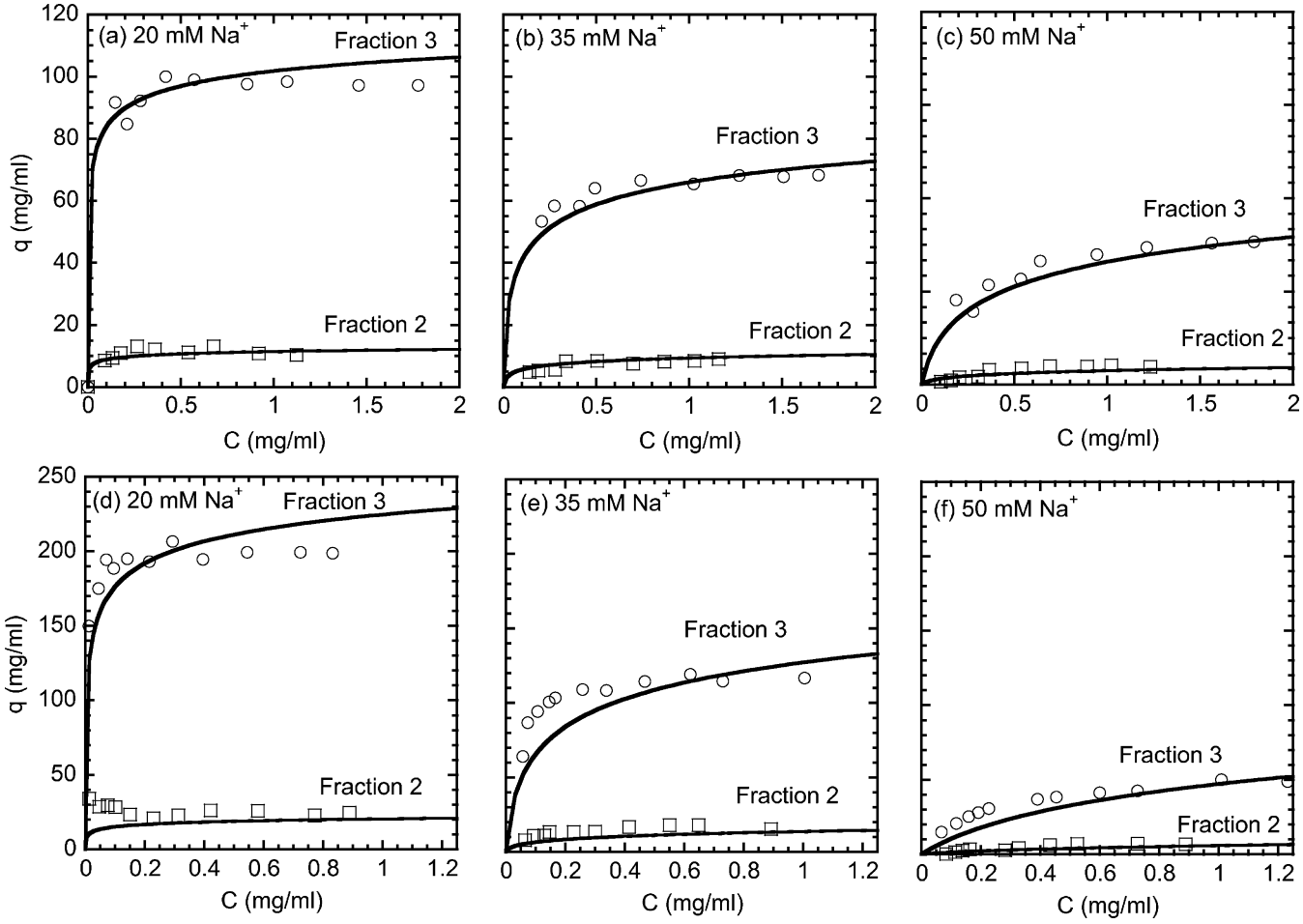

Fig. 9. Two-component adsorption isotherms for mixtures of mAb fractions 2 and 3 at pH 7.5 on UNOsphere S (a–c) and Capto S (d–f). Lines are predictions based on the SMA isotherm model using the parameters in Table 3. Note that different vertical scales have been used for UNOsphere S and Capto S.

Table 4
Comparison of experimental and predicted multicomponent adsorption at pH 7.5 for different initial ratios of the deamidated isoforms and 20 mM Na^+. Predictions are based on the SMA model with isotherm parameters in Table 3.

Initial ratio	C_1 (mg/ml)		C_2 (mg/ml)		C_3 (mg/ml)		q_1 (mg/ml)		q_2 (mg/ml)		q_3 (mg/ml)	
	Exp.	Pred.	Exp.	Pred.	Exp.	Pred.	Exp.	Pred.	Exp.	Pred.	Exp.	Pred.
UNOsphere S												
3:1	–	–	1.1	1.1	0.10	0.13			57	61	46	43
1:1	–	–	0.88	0.87	0.38	0.38			25	30	75	78
1:3			0.48	0.44	0.69	0.73			5.1	10	107	101
1:1:2	0.46	0.44	0.42	0.40	0.43	0.45	2.6	2.1	15	14	90	92
Capto S												
3:1			1.1	0.96	0.06	0.08			114	128	98	84
1:1			0.80	0.78	0.35	0.25			68	65	153	159
1:3			0.43	0.43	0.51	0.57			20	22	215	216
1:1:2	0.43	0.45	0.39	0.41	0.40	0.41	12	5.8	30	26	190	199

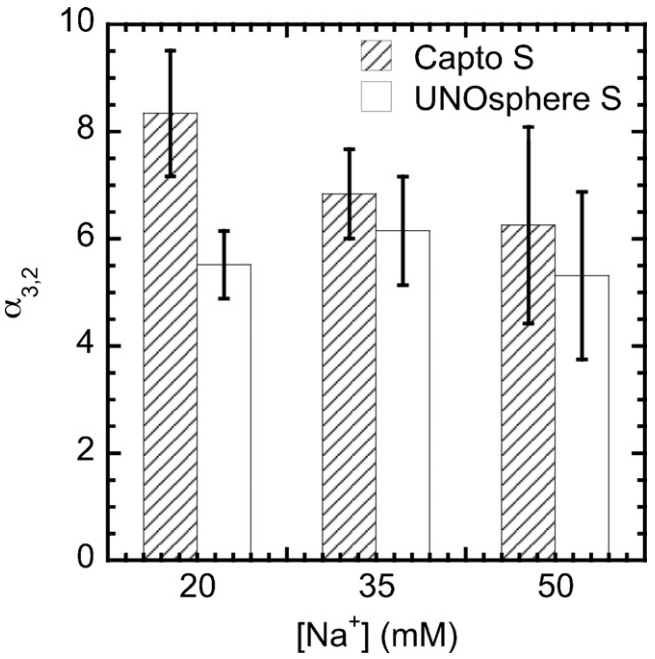

Fig. 10. Experimental selectivities between mAb variants 3 and 2 at pH 7.5 and different Na^+ concentrations. Error bars indicate the range of α-values obtained at different protein concentrations.

combining Eq. (2) with the following material balances:

$$q_i = \frac{V}{V_M}(C_i^0 - C_i) \quad \text{for } i = 1, n \tag{7}$$

where V and V_M are the solution and particle volumes, respectively, and C_i^0 is the initial fluid phase concentration. The resulting system of equations was solved using the Newton–Raphson method. Predictions using the parameters determined for the single component isotherms are shown in Fig. 9 and Table 4. As seen from these results, the SMA model provided a reasonably accurate and thermodynamically consistent prediction of the two-component results with average relative deviation of ±5.2%, ±21%, and ±35% for mAb fraction 3, 2, and 1, respectively in two and three component mixtures. Accordingly, since the values of z and σ were statistically the same for all three mAb variants, the selectivity

$$\alpha_{i,j} = \frac{q_i}{q_j}\frac{C_j}{C_i} = \frac{K_{e,i}}{K_{e,j}} \tag{8}$$

was predicted to be a constant equal to the ratio of the respective K_e-values and independent of salt and protein concentration. The calculated values at pH 7.5 based on the isotherm data are $\alpha_{3,2} = 4.2 \pm 0.8$ and $\alpha_{2,1} = 8.6 \pm 1.2$ for UNOsphere S and $\alpha_{3,2} = 4.9 \pm 0.8$ and $\alpha_{2,1} = 13 \pm 2$ for Capto S. Experimental values of $\alpha_{3,2}$ are shown in Fig. 10 for a range of salt and protein concentrations. It can be seen that selectivity differences between the two media were small and significant only at the lowest Na^+ concentration.

4. Conclusions

We have examined the adsorption of deamidated mAb variants on two commercial cation exchange media – one with open pore architecture and the other with charged dextran grafts. Binding capacities were higher at pH 5 compared to pH 7.5. However, no selectivity between the deamidated forms was observed at pH 5. On the other hand, at pH 7.5, while binding was weaker, both media preferentially adsorbed the less deamidated forms. At low ionic strengths the binding capacity was substantially higher for the dextran-grafted matrix Capto S despite the fact that in iSEC experiments this material excluded neutral dextran probes with molecular mass larger than 10 kDa. This result suggests that mAb binding was influenced by strong, multivalent interactions with the functional dextran grafts incorporated in this material. At higher ionic strengths, the situation was reversed. mAb binding became stronger for the open pore media when the ionic strength was 140 mM (conductivity ~15 mS/cm) at pH 5 and when the ionic strength was 50 mM (conductivity ~5 mS/cm) at pH 7.5.

The values of the effective binding charge for the SMA model were around 7 for the open pore matrix and around 8.3 for the dextran-grafted media. These fitted z-values did not change when the pH was reduced to 5 indicating that the protein interacted with the adsorbent surface similarly at the two pH conditions independently of the net charge, which was different for the different deamidated mAbs and substantially higher at the lower pH. Conversely, different equilibrium binding constants, $K_{e,i}$, were obtained for the different deamidated forms suggesting that the binding strength was affected by the net charge. The SMA hindrance factor, σ, representing the number of surface-bound ligands shielded by the bound protein molecules, was also determined. This value was the same for the different mAb forms but was lower for the dextran-grafted media Capto S suggesting that the charged functional groups in this matrix were shielded to a lesser extent. Since the z and σ-values were the same for the different mAb forms, the selectivity was constant for our system and independent of salt and protein concentration.

Beside offering the ability of correlating the effects of salt on the binding capacity, the SMA model could also successfully predict two- and three-component adsorption equilibria for both stationary phases thereby providing a valuable tool for the design and optimization of actual charge variant chromatographic separation processes.

Acknowledgement

This research was supported by MedImmune and NSF Grants No. CTS-0729857 and CBET-1032727.

References

[1] M. Perkins, R. Theiler, S. Lunte, M. Jeschke, Pharmaceut. Res. 17 (2000) 1110.
[2] D. Chelius, D.S. Rehder, P.V. Bondarenko, Anal. Chem. 77 (2005) 6004.
[3] G.G. Bulseco, B. Li, A. Bulseco, H. Liu, Anal. Chem. 80 (2008) 9491.
[4] J. Cacia, R. Keck, L.G. Presta, J. Frenz, Biochemistry 35 (1996) 1897.
[5] Y.R. Hsu, W.C. Chang, E.A. Mendiaz, S. Hara, D.T. Chow, M.B. Mann, K.E. Langley, H.S. Lu, Biochemistry 37 (1998) 2251.
[6] N.E. Robinson, K.J. Lampi, R.H. Williams, G. Kruppa, A.B. Robinson, Mol. Vis. 11 (2005) 1211.
[7] D. Prome, J.C. Prome, C. Deon, P. Groff, G. Kalmes, F. Galacteros, H. Wajcman, J. Mass Spectrom. (Suppl. S) (1995) S165.
[8] K.G. Moorhouse, W. Nashabeh, J. Deveney, N.S. Bjork, M.G. Mulkerrin, T. Ryskamp, J. Pharm. Biomed. Anal. 16 (1997) 593.
[9] L. Melter, G. Ströhlein, A. Butté, M. Morbidelli, J. Chromatogr. A 1154 (2007) 121.
[10] A.W. Yem, K.A. Richard, N.D. Staite Jr., M.R. Deibel, Lymphokine Res. 7 (1988) 85.
[11] T. Adachi, H. Takayanagi, A.D. Sharpe, J. Chromatogr. A 763 (1997) 57.
[12] M. Weitzhandler, D. Farnan, J. Horvath, J.S. Rohrer, R.W. Slingsby, N. Advalovic, C. Pohl, J. Chromatogr. A 828 (1998) 365.
[13] R.J. Harris, B. Kabakoff, F.D. Macchi, F.J. Shen, M. Kwong, J.D. Andya, S.J. Shire, N. Bjork, K. Totpal, A.B. Chen, J. Chromatogr. B 752 (2001) 233.
[14] G.L. Skidmore, H.A. Chase, J. Chromatogr. 505 (1990) 329.
[15] R.K. Lewus, G. Carta, AIChE J. 45 (1999) 512.
[16] C.A. Brooks, S.M. Cramer, AIChE J. 38 (1992) 1969.
[17] G. Garke, R. Hartmann, N. Papamichael, W.D. Deckwer, F.B. Anspach, Sep. Sci. Technol. 34 (1999) 2521.
[18] T. Gu, G.-J. Tsai, G.T. Tsao, AIChE J. 37 (1991) 1333.
[19] M.M.H. El-Sayed, H.A. Chase, Biochem. Eng. J. 49 (2010) 221.
[20] X. Xu, A.M. Lenhoff, J. Chromatogr. A 1216 (2009) 6177.
[21] B.D. Bowes, H. Koku, A.M. Lenhoff, Protein retention and transport in polymer-modified ion-exchange media, in: Paper Presented at the 13th

International Symposium on Preparative and Industrial Chromatography and Allied Techniques, SPICA 2010, Stockholm, Sweden, September, 2010.
[22] Y. Tao, G. Carta, J. Chromatogr. A 1211 (2008) 70.
[23] M.C. Stone, G. Carta, J. Chromatogr. A 1116 (2007) 206.
[24] A. Ubiera, G. Carta, Biotechnol. J. 1 (2006) 665.
[25] L. Hagel, M. Ostberg, T. Andersson, J. Chromatogr. A 743 (1996) 33.
[26] J. Vlasak, M.C. Bussat, S. Wang, E. Wagner-Rousset, M. Schaefer, C. Klinguer-Hamour, M. Kirchmeier, N. Corvaïa, R. Ionescu, A. Beck, Anal. Biochem. 392 (2009) 145.
[27] N. Forrer, A. Butté, M. Morbidelli, J. Chromatogr. A 1214 (2008) 59.
[28] K. Rege, N. Tugcu, S.M. Cramer, Sep. Sci. Technol. 38 (2003) 1499.
[29] G. Carta, A.R. Ubiera, T.M. Pabst, Chem. Eng. Technol. 28 (2005) 1252.